

Comprehensive Analysis of Nanostructure of Oxide Dispersion-Strengthened Steels by Ultramicroscopy Methods

S. V. Rogozhkin^{a, b, *, **}, A. A. Khomich^{a, b}, A. V. Klauz^{a, b}, A. A. Bogachev^{a, b}, Y. E. Gorshkova^c, G. D. Bokuchava^c, A. A. Nikitin^{a, b}, A. A. Lukyanchuk^{a, b}, O. A. Raznitsyn^{a, b}, A. S. Shutov^{a, b}, and A. G. Zaluzhny^{a, b}

^a National Research Nuclear University “MEPhI,” Moscow, 115409 Russia

^b NRC “Kurchatov Institute,” Kurchatov Complex for Theoretical and Experimental Physics, Moscow, 123182 Russia

^c Joint Institute for Nuclear Research, Dubna, 141980 Russia

*e-mail: Sergey.Rogozhkin@itep.ru

**e-mail: SVRogozhkin@mephi.ru

Received May 31, 2022; revised June 20, 2022; accepted June 20, 2022

Abstract—The characterization of the nanostructure of modern oxide dispersion strengthened steels requires a comprehensive analysis using complementary techniques. In this work, the methods of small-angle X-ray scattering, transmission electron microscopy and atom probe tomography have been applied to several oxide dispersion strengthened steels. Comparison of the obtained results allows the most correct characterization of inclusion types and their number in the studied materials. It is shown that most of the studied steels contain oxide inclusions and nanosized clusters enriched in O and Y, as well as V, Ti, Al, and Zr, depending on the initial steel composition. Transmission electron microscopy and atom probe tomography provide detailed information about the inclusion types, and small-angle X-ray scattering gives the most accurate estimation of the average density of inclusions in large volumes of material. The importance of the correct determination of the inclusion types for hardening calculations is shown, the results of such calculations are compared with microhardness measurements. The calculated values of hardness for the studied steels are in the range 2.7–4.3 GPa, which is well confirmed by microhardness measurements.

Keywords: oxide dispersion strengthened steel, small-angle X-ray scattering, transmission electron microscopy, atom probe tomography, oxide particle, nanocluster, microhardness, dispersed barrier hardening model

DOI: 10.1134/S1027451022060490

INTRODUCTION

Currently, various nanostructured materials are being developed. Nanostructured oxide dispersion-strengthened (ODS) alloys and steels show a much higher heat resistance compared to conventional materials (base alloys without oxide inclusions) due to a significant number of uniformly distributed oxide inclusions (for example, [1]). The areas of applications of these materials are quite different: from gas-turbine engines to the core of nuclear power plants. The development of these materials includes improving the structural phase state, such as reducing the grain size, optimizing the size and composition of the contained inclusions, as well as the uniformity of their distribution throughout the material volume. The characterization of nanostructure of modern ODS alloys requires a comprehensive analysis using complementary techniques.

The combination of atom probe tomography and transmission electron microscopy makes it possible to study the structure of a material in a wide range of spa-

tial scales: from nanoscale clusters to microstructure [2]. At the same time, both methods are local and do not provide information about a larger volume of the material under study. Additional methods, such as small-angle X-ray scattering [3] or small-angle neutron scattering [4], are necessary to obtain information about the average characteristics of a nanostructure in a large volume of material. The aim of this work was a comprehensive analysis of the nanostructure of ODS steels using transmission electron microscopy (TEM), atom probe tomography (APT), and small-angle X-ray scattering (SAXS), as well as an evaluation of the contribution of various features of the nanostructure to the strengthening of ODS steels. For these calculations, the dispersed barrier hardening model (DBH) was used.

MATERIALS AND METHODS

The materials for this study are Eurofer ODS (EU-Charge) and Austenitic ODS developed at the Karl-

Table 1. Chemical composition of the investigated ODS steels (at %)

Steel	Fe	Mo	Al	Ni	Zr	Mn	Cr	W	Y	O	Ti	V	C	N	Ar	Si
Eurofer ODS	88.08	—	—	0.02	—	0.39	9.81	0.34	0.13	0.34	—	0.22	0.40	0.21	—	0.06
10Cr ODS	86.90	0.57	—	—	—	0.50	10.64	—	0.17	0.17	0.29	0.11	0.60	0.02	0.01	—
14Cr ODS	84.65	—	—	—	—	—	14.44	0.33	0.12	0.12	0.23	—	0.05	0.03	—	0.01
Austenitic ODS	67.78	—	—	14.29	—	—	15.84	0.43	0.16	0.35	0.17	0.11	0.46	0.40	—	—
KP-1 ODS	77.24	—	6.42	—	0.28	—	15.13	0.56	0.16	0.04	—	—	0.13	0.02	0.01	—
KP-3 ODS	78.29	—	6.40	—	—	—	13.82	0.55	0.16	0.37	0.18	—	0.21	—	—	—
KP-4 ODS	74.92	—	7.57	—	0.28	—	15.46	0.53	0.16	0.63	0.13	—	0.27	0.02	0.01	—

ruhe Institute of Technology (KIT, Germany), KP ODS steels developed at the Kyoto University (Japan), 10Cr ODS developed at the Korean Atomic Energy Institute (KAERI, Republic of Korea) and 14Cr ODS developed by the French Alternative and Atomic Energy Commission (CEA) (France). All studied ODS steels were produced by mechanical alloying of metal powders with Y_2O_3 powders. The chemical compositions of the studied steels are presented in Table 1. Eurofer ODS and 10Cr ODS steels contain ~10 at % chromium. Austenitic ODS and KP steels belong to high chromium steels (~14–16 at %). Yttrium and oxygen are considered to be the main elements in formation of the ODS steel structure. The yttrium content in the studied steels is in the range 0.12–0.17 at %, and the oxygen content is in the range 0.12–0.63 at %. These steels also differ in the content of V, Ti, Zr and Al, their role will be discussed later.

There are also differences in the thermomechanical treatment of the studied steels. KP ODS steels were encapsulated in mild steel and degassed in vacuum at a pressure of 10^{-3} Torr at 400°C for 3 h. Next, hot extrusion was performed at 1150°C to shape the steel into a rod with a diameter of 25 mm, followed by annealing at 1150°C in vacuum for 1 h and subsequent cooling in air. The 10Cr ODS steel was first subjected to hot isostatic pressing at 1150°C for 4 h at 100 MPa, followed by hot rolling at 1100°C, normalization at 1050°C for 1 h with subsequent air cooling and tempering at 780°C for 1 h followed by air cooling. The 14Cr ODS steel was hot-rolled from 125 to 63 mm, then heated to 1100°C, and then hot-rolled several times to a thickness of 2 mm. Eurofer ODS steel was normalized at 1100°C for 30 min with water quench followed by tempering at 750°C for 2 h and air cooling. Austenitic ODS steel was subjected to hot isostatic pressing at 100 MPa at 900°C for 1 h without any subsequent heat treatment.

The phase composition of ODS steels was analyzed using TEM, electron diffraction, and scanning transmission electron microscopy. To obtain microphotographs in the Z-contrast mode, a Titan 80-300 S/TEM microscope (Thermo Fisher Scientific, USA) with an accelerating voltage of 300 kV equipped with a ring high-angle dark-field detector (HAADF, Fischione) was

used. Using a combination of these techniques, the characteristic sizes of grains and different type inclusions were determined. To obtain inclusion size distributions, statistics were collected on more than 2000 detected objects. The average size of inclusions, their number density, and the standard deviation of size values were determined from the obtained size distributions. The error in determining the number density of inclusions was calculated based on the combination of errors in measuring the studied layer thickness and the microscope resolution, as well as the scatter of values between the studied volumes.

Samples for microscopic investigations by TEM were prepared by the focused beam of Ga^+ ions using a dual-beam scanning electron microscope HELIOS NanoLab 600 (FEI, Holland) at an accelerating voltage of 5–30 kV. To reduce the thickness of the damaged amorphous layer due to interaction with the ion beam, additional thinning was performed at an accelerating voltage of 2 kV. For TEM studies, thin cross-section samples were prepared. The volumes of each material with a total number of oxide inclusions of at least 2000 were studied.

The nanostructure of ODS steels was investigated using an APPLE-3D tomographic atom probe with femtosecond laser evaporation, developed at the Institute of Theoretical and Experimental Physics (Moscow) [5]. Data was collected at a reference sample temperature of 40–50 K in the laser evaporation mode with a wavelength of 515 nm, a laser pulse duration of 300 fs, a frequency of 25 kHz, and a pulse energy of 0.1–1.2 μJ [6]. The pressure in the research chamber was $(5-7) \times 10^{-10}$ Torr.

To prepare samples for APT, pre-samples $0.3 \times 0.3 \times 10$ mm in size were prepared from the initial ingots by electroerosion cutting in water. Further thinning of the pre-samples was carried out by standard methods of electrochemical anodic electropolishing to form the tip of the sample with a rounding radius of 15–50 nm. The needle-samples obtained were quality-controlled using a JEOL 1200 EX transmission electron microscope.

At least two volumes of each material with dimensions of $30 \times 30 \times 300$ nm were examined by APT. Reconstruction and analysis of APT data included the

mass spectrum interpretation and characterization of three-dimensional distributions of chemical elements in the studied volumes using the KVANTM-3D software package [7]. To reconstruct 3D atom maps, the general Bass reconstruction method [8] was used, in which the back projection of each detected ion was calculated using the radius of the sample tip and the distance between the sample and the detector.

Nanoscale inclusions detected by APT are usually called clusters, their specific feature is the enrichment in some elements in comparison with the material matrix. A maximum separation algorithm was used to characterize nanoscale features (clusters). This algorithm depends on two main parameters: the search sphere diameter d_{\max} and the threshold value N_{\min} . The first determines the search area of the proposed cluster, and the second acts as a threshold for the cluster presence in a given area. A detailed description of this algorithm is given in [9, 10]. In this work, to search for cluster, the elements Y, O, Ti, V, and Zr were chosen depending on the steel composition and the cluster enrichment with these elements. The cluster search parameters d_{\max} and N_{\min} were 0.7 nm and seven atoms for Austenitic ODS, 0.7 nm and six atoms for 14Cr ODS, 0.5 nm and six atoms for Eurofer ODS, 0.7 nm and six atoms for KR-3 ODS, 0.6 nm and eight atoms for KR-1 ODS, and 0.6 nm and nine atoms for KR-4 ODS, respectively. Based on the principle of ignoring random fluctuations, the minimum number of atoms in a cluster was chosen to be 50. To obtain the cluster size distributions, statistics were collected for more than 30 objects. The average cluster size and the scatter of size values were determined based on the total volume of all studied samples and the total number of clusters. The number density error was determined from the deviations of the examined volumes from the average value.

SAXS measurements were performed on a SAXS/WAXS Xeuss 3.0 station (Xenocs, France) operating in point geometry using a GeniX3D microfocus X-ray source tube with Mo $K_{\alpha 1}$ emission ($\lambda = 0.0709$ nm) in the 30 W/30 μm mode. The spectrometer is equipped with an Eiger2 R 1M moving detector with a sensitive area of 77.1×79.7 mm² (pixel size 75 μm). SAXS measurements were carried out in vacuum at room temperature at a distance of 350 mm from the sample to the detector, which allowed us to measure the X-ray scattering intensity $I(Q)$ in the transmitted pulse range $0.01 < Q < 0.16$ nm⁻¹ ($Q = (4\pi/\lambda)\sin(\theta/2)$), where λ is the wavelength of the incident radiation, and θ is the scattering angle).

To carry out SAXS measurements, the samples of ODS steels were prepared in the form of disks 3 mm in diameter and 100 μm thick. For each material, measurements were carried out on two samples. The scattering curves were approximated by a function consisting of two terms [11]. The first term is the Porod behavior in the range of small Q -values, correspond-

ing to the power law of scattering at sharp boundaries of large-scale grains of the material, and the second term corresponds to scattering by small spherical inclusion particles with radius R :

$$I(Q) = A Q^{-4} + N \left(3V\Delta\rho \frac{\sin(QR) - QR\cos(QR)}{(QR)^3} \right)^2 + C, \quad (1)$$

where A is a constant, N is the particle number density, R is the radius of a spherical particle, $V = \frac{4}{3}\pi R^3$ is the volume of an individual particle, $\Delta\rho$ is the scattering length density difference (contrast) between the matrix and particle, C is the incoherent background.

The experimental SAXS data were approximated by the least-squares method according to the described model (1) using the SasView program [12]. In accordance with the generally accepted approach, the lognormal particle radius distribution was used in the model to correctly take into account the polydispersity of the system and to appropriately fit the SAXS curve profiles. Structural parameters were the particle number density N and their average size $D = 2R$. The size dispersion was calculated using the standard deviation of the inclusion sizes from their average value.

RESULTS OF MICROSCOPY ANALYSIS

TEM analysis of ODS steels showed that all steels contained inclusions uniformly distributed over grains. A complete microstructural analysis of these steels was carried out earlier [2] and was also described in [13–18]. It should be noted that the most of the detected inclusions larger than 5 nm had the structure of various oxides. Steels with Ti content (Austenitic ODS, 10Cr ODS and 14Cr ODS) contained $\text{Y}_2\text{Ti}_2\text{O}_7$ or Y_2TiO_5 oxides. Steels containing Al (KP-1, KP-3, KP-4) had $\text{Y}_4\text{Al}_2\text{O}_9$, YAlO_3 , or $\text{Y}_3\text{Al}_5\text{O}_{12}$ inclusions. The KP-1 and KP-4 steels containing Zr had $\text{Y}_4\text{Zr}_3\text{O}_{12}$ or $\text{Y}_2\text{Zr}_2\text{O}_7$ oxides. Only Eurofer ODS steel contained Y_2O_3 oxides. The stoichiometry of inclusions smaller than 5 nm is quite difficult to detect. However, these small oxide inclusions were enriched in the same chemical elements (Y–Ti–O, Y–Al–O, Y–Zr–O, and Y–O) as the large oxides in these steels. From this point, the term “oxide inclusions” will be used for inclusions observed by TEM in ODS steels. The characteristic grain sizes are summarized in Table 2. The size distributions of oxide inclusions in various steels are shown in Fig. 1. The average sizes and number densities of particles detected in TEM are shown in Fig. 2. Most of the detected inclusion are 2–10 nm in size.

The highest number density of oxide inclusions ($13 \times 10^{22} \text{ m}^{-3}$) was found in 10Cr ODS with the highest Ti content (0.29 at %), as well as with 0.11 at % V and 0.5 at % Mn. A slightly lower density of oxide

Table 2. Average size and number density of objects detected in the studied ODS steels by the TEM, APT and SAXS methods

Steel	TEM			APT		SAXS	
	grain size, μm	average size, nm	number density, 10^{22} m^{-3}	average size, nm	number density, 10^{22} m^{-3}	average size, nm	number density, 10^{22} m^{-3}
Eurofer ODS	0.3–2	6 ± 2	4 ± 1	3 ± 1	10 ± 3	2.8 ± 0.6	16 ± 8
10Cr ODS	0.2–1.5	3 ± 1	13 ± 2	4 ± 1	9 ± 1	2.7 ± 0.1	27 ± 5
14Cr ODS	$(1-6) \times (0.05-0.35)$	4 ± 1	2 ± 1	4 ± 2	41 ± 5	1.3 ± 0.3	35 ± 8
Austenitic ODS	0.1–0.5	6 ± 2	2 ± 1	4 ± 1	28 ± 4	2.7 ± 0.1	32 ± 9
KP-3 ODS	0.5–2	3 ± 1	4 ± 1	4 ± 1	13 ± 2	3.2 ± 0.1	6 ± 3
KP-1 ODS	0.6–2	8 ± 3	2 ± 1	9 ± 1	1.5 ± 0.6	5.4 ± 1.0	1.4 ± 0.3
KP-4 ODS	0.5–1.5	5 ± 1	4 ± 1	4 ± 1	9 ± 3	5.3 ± 0.2	2 ± 1

inclusions ($9 \times 10^{22} \text{ m}^{-3}$) was detected in KP-3 ODS with 0.18 at % Ti, 0.55 at % W, 0.22 at % Zr, and even lower in Eurofer ODS with 0.22 at % V without Ti. The lowest number density was in KP-1 ODS without Ti, V, and Mn, but with 0.22 at % Zr. At the same time, Austenitic ODS and 14Cr ODS also had the minimum number of inclusions, although they contained 0.17 and 0.23 at % Ti, respectively.

An analysis of ODS steels by APT also revealed a significant number of nanoscale inclusions (oxide clusters). All detected clusters are enriched in Y and O (Fig. 3). In all steels containing titanium, the clusters are also enriched in Ti, and in all steels with vanadium (Eurofer ODS, 10Cr ODS and Austenitic ODS), the clusters are also enriched in V. Titanium is absent in clusters only in Eurofer ODS steel, which lacks titanium. Vanadium enriches the clusters in vanadium containing steels Eurofer ODS, 10Cr ODS and Austenitic ODS. Aluminum is a cluster enrichment element only in KP-3 ODS steel. In the KP-1 ODS and KP-4 ODS steels which containing Zr in addition to Al, the clusters are depleted in Al and, additionally, enriched in zirconium. In all zirconium-free steels, the clusters are also enriched in chromium. A thorough representation of the cluster enrichment (the excess of the concentration of chemical elements in clusters over their concentration in the matrix) for all ODS steels studied is shown in Fig. 3 (a negative value on the graph corresponds to depletion of a specific element).

Cluster size distributions are shown in Fig. 4. The average cluster sizes and number density are shown in Fig. 5. Generally, the clusters are 3–5 nm in size, only in KP-1 ODS steel their characteristic sizes are 8–10 nm. And it is in this case the lowest number density of clusters was observed. The highest number density of clusters (more than 10^{23} m^{-3}) was found in Austenitic ODS and 14Cr ODS steels.

SAXS does not allow one to determine the nature of observed inclusions (it cannot distinguish oxide inclusions from clusters), but it makes it possible to obtain their average characteristics for macroscopic volumes of material. Figure 6 shows the average sizes and number densities obtained from two independent measurements. Figure 7 presents the size distributions of the inclusions (from one measurement) obtained by SAXS. The difference between the average sizes obtained from different measurements was taken into account by averaging with the use of weight coefficients that take into account the density of the detected objects.

COMPARISON OF THE RESULTS OBTAINED BY DIFFERENT ULTRAMICROSCOPY TECHNIQUES

Average sizes and number densities of objects detected by APT, TEM, and SAXS methods are listed in Table 2. In order to analyze this data, several factors must be taken into account. TEM and APT are local analysis methods that allow detailed analysis of one or more grains. At the same time, TEM makes it possible to detect secondary phases quite well in a wide range of sizes, but it has some problems with the identification of inclusions of a complex chemical composition with a size of a few nanometers. APT detects nanometer inclusions with the highest detail of the distribution of atoms of chemical elements in them, but examines a noticeably smaller volume compared to TEM. The difficult point is that the objects observed by TEM and APT can be either different or coincide, which requires the use of additional methods of analysis for obtaining the integral characteristics of inclusions in ODS steels. SAXS is unable to determine the differences in the chemical composition of inclusions, but it analyzes the macroscopic region of the material (thickness $\sim 100 \mu\text{m}$), which is much larger than the

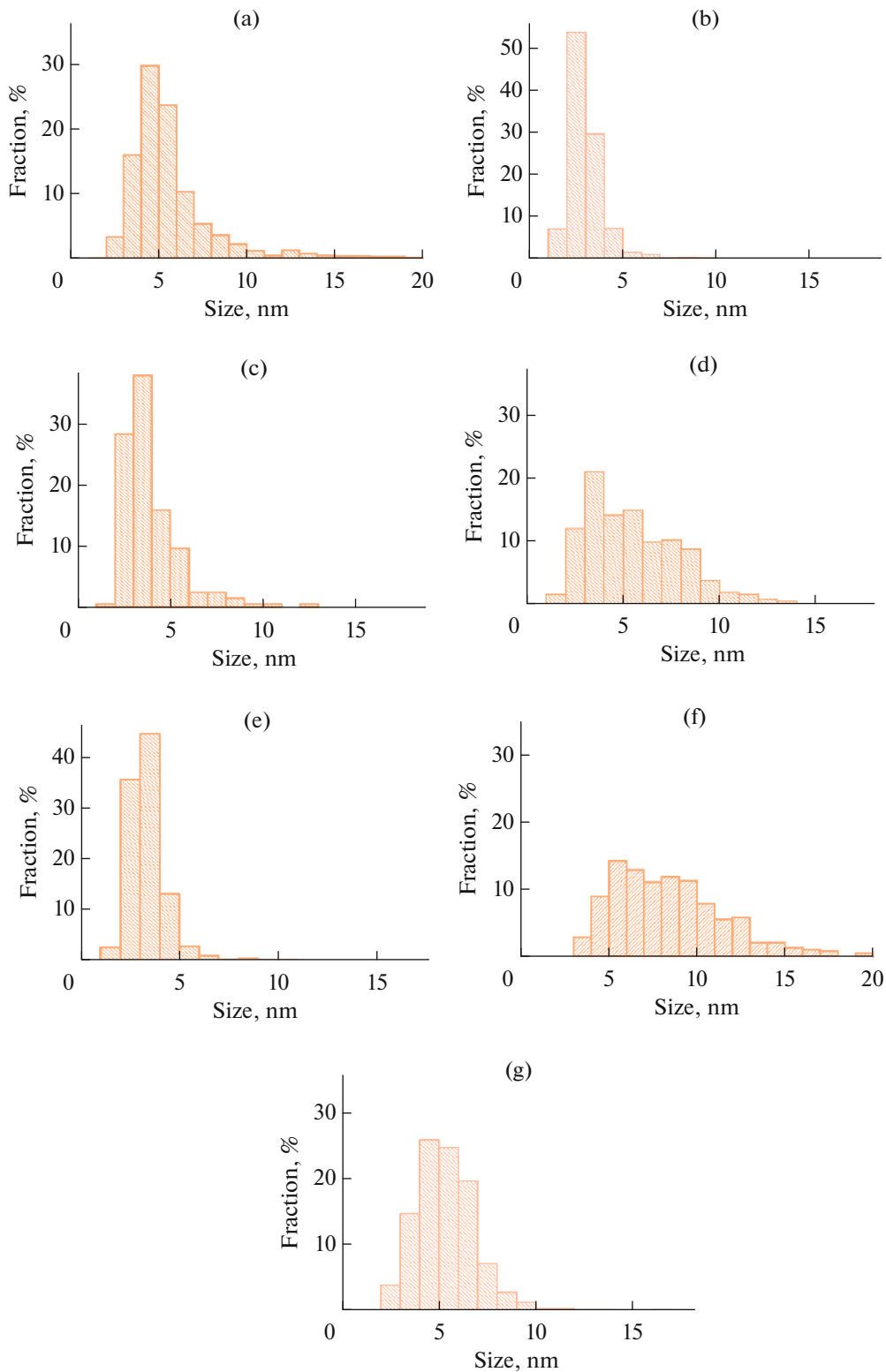


Fig. 1. Size distribution of TEM-detected oxide inclusions in ODS steels: (a) Eurofer ODS; (b) 10Cr ODS; (c) 14Cr ODS; (d) Austenitic ODS; (e) KP-3 ODS; (f) KP-1 ODS; (g) KP-4 ODS.

study area of TEM and APT local methods. This SAXS feature makes it possible to determine the macroscopic average characteristics of inclusions with

high accuracy. Comparison of the data obtained by three different methods allows us to divide the studied materials into several groups. In Eurofer ODS steel,

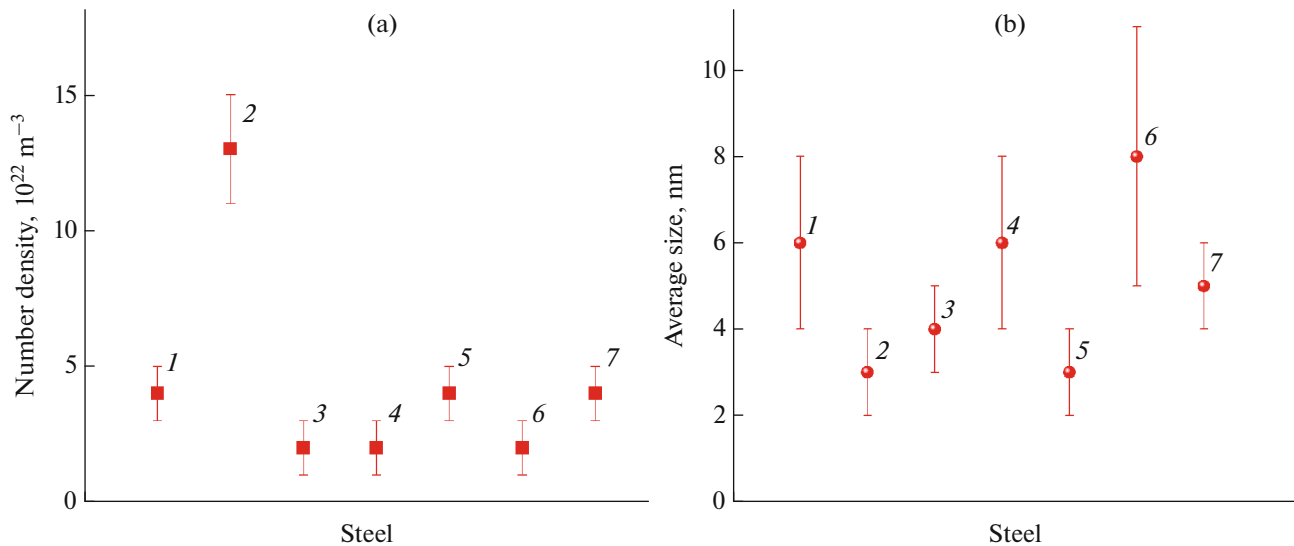


Fig. 2. (a) Number density and (b) average size of TEM-detected oxide inclusions in ODS steels: Eurofer ODS (1); 10Cr ODS (2); 14Cr ODS (3); Austenitic ODS (4); KP-3 ODS (5); KP-1 ODS (6); KP-4 ODS (7).

the sizes of oxide inclusions observed by TEM and clusters observed by APT are clearly different. Austenitic ODS steel shows a similar behavior. For these steels, the inclusion density determined by SAXS can be considered within errors as the sum of the number densities of oxide inclusions and clusters, which indicates a clear difference between the objects detected by TEM and APT. For all other steels, there is a clear overlap in the sizes of oxide inclusions and clusters, which makes it impossible to separate these objects. That means that there is a high probability of observing the same objects with TEM and APT. At the same time, in 10Cr ODS and 14Cr ODS steels, the total density of inclusions observed by SAXS methods, taking into account possible errors, is also most likely the sum of the densities of oxide inclusions and clusters. The same objects were detected by TEM and APT only in KP ODS steels, because both the sizes and number densities of these objects were close to each other and close to the SAXS data.

Note that in 14Cr ODS steel and Austenitic ODS, the number density of clusters exceeds the density of oxide inclusions by more than 10 times, which indicates that the average characteristics of inclusions will be determined by the objects observed in APT. In Eurofer ODS steel, the situation is similar: the number density of clusters exceeds the density of oxide inclusions by a factor of two. And, as a consequence, despite the fact that the sizes of oxide inclusions are two times larger than those of oxide clusters, the SAXS data is quite close to the results of APT.

COMPARISON OF DBH MODEL CALCULATIONS WITH RESULTS OF EXPERIMENTAL MEASUREMENTS

The data obtained from a comprehensive analysis of the structural-phase state of ODS steels allows to estimate the contribution of detected inclusions to hardening. DBH model was used to estimate the yield strength [19]. Within this model, each barrier type contributes to hardening according to the Orowan formula:

$$\Delta\sigma_i = M_T \alpha_i \mu b \sqrt{N_i d_i}, \quad (2)$$

where α_i is the barrier strength; M_T is the Taylor factor; μ is the shear module; b is the Burgers vector modulus; N_i and d_i are number density and average size of this barrier type, respectively. The barrier values α_i are different for oxide inclusions and clusters. For calculations, the coefficients $\alpha_c = 0.1$ for clusters [20] and $\alpha_o = 0.63$ for oxide inclusions were chosen [21].

In addition to small particles, the contribution to the total hardening of the material is made by grain boundaries and the matrix. Strengthening due to the grain boundaries is determined by the well-known Hall–Petch relation:

$$\sigma_{gb} = kD^{-1/2}, \quad (3)$$

where D is the grain size and $k = 338 \text{ MPa}/\mu\text{m}$. Solid-phase hardening is accepted for ferritic-martensitic steels [22] $\sigma_m = 0.255 \text{ GPa}$ and for austenitic steels $\sigma_m = 0.3 \text{ GPa}$ [23].

The total hardening from all barrier types was calculated by the formula (for example, [1]):

$$\sigma_y = \sqrt{\sigma_c^2 + \sigma_o^2} + \sigma_m + \sigma_{gb}, \quad (4)$$

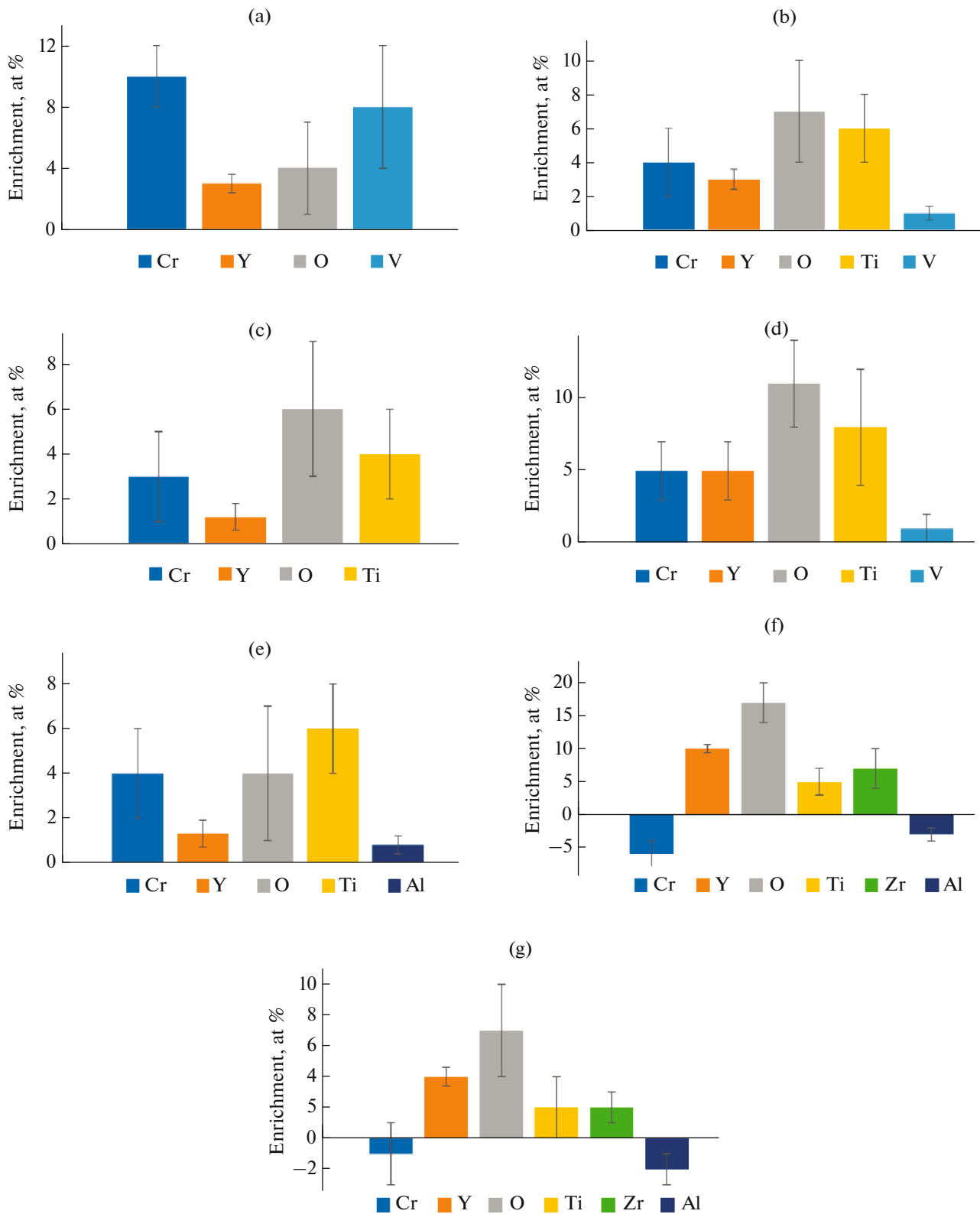


Fig. 3. Enrichment of APT-detected clusters in the ODS steels: (a) Eurofer ODS; (b) 10Cr ODS; (c) 14Cr ODS; (d) Austenitic ODS; (e) KP-3 ODS; (f) KP-1 ODS; (g) KP-4 ODS.

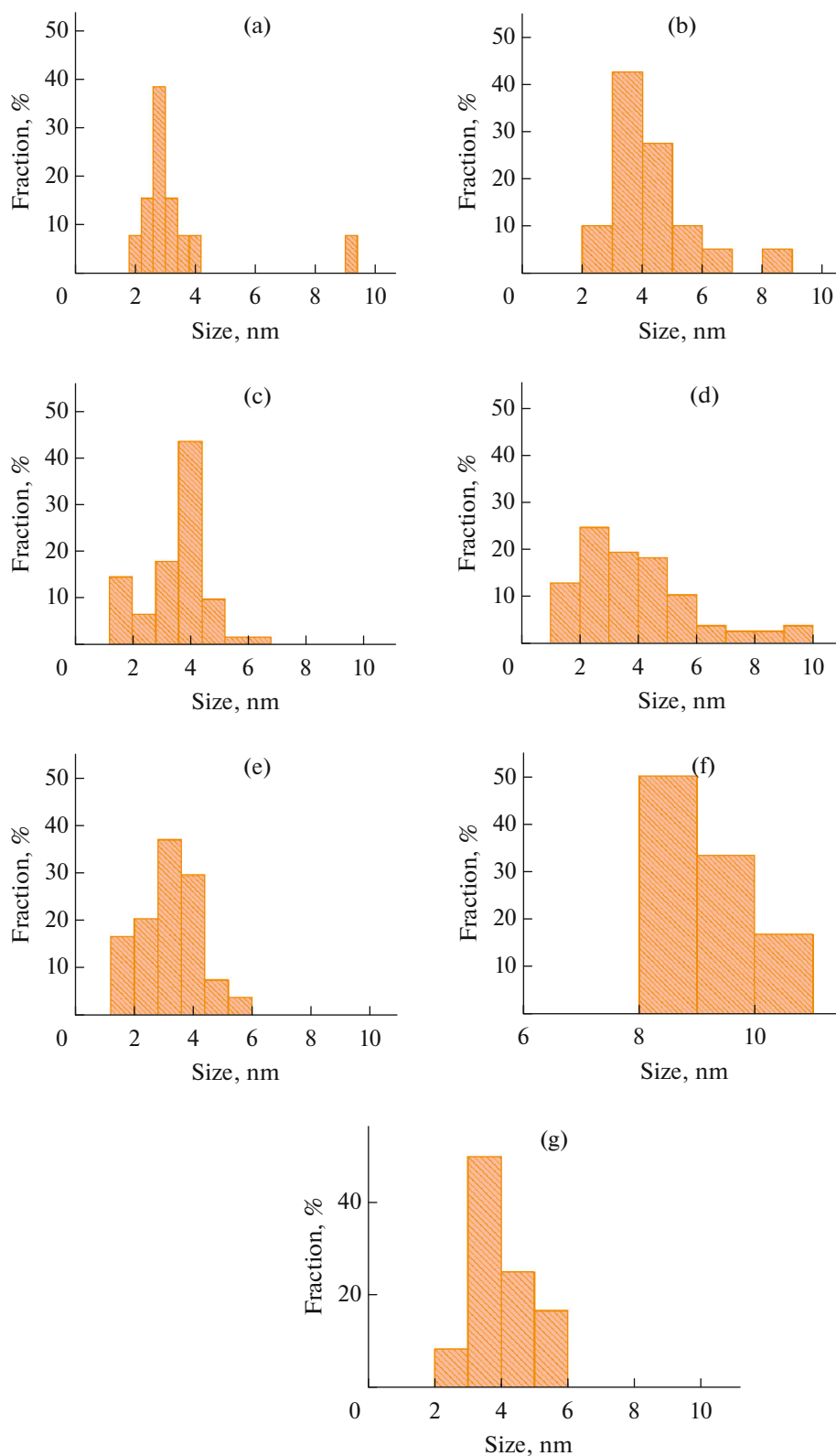


Fig. 4. Size distribution of APT-detected oxide clusters in ODS steels: (a) Eurofer ODS; (b) 10Cr ODS; (c) 14Cr ODS; (d) Austenitic ODS; (e) KP-3 ODS; (f) KP-1 ODS; (g) KP-4 ODS.

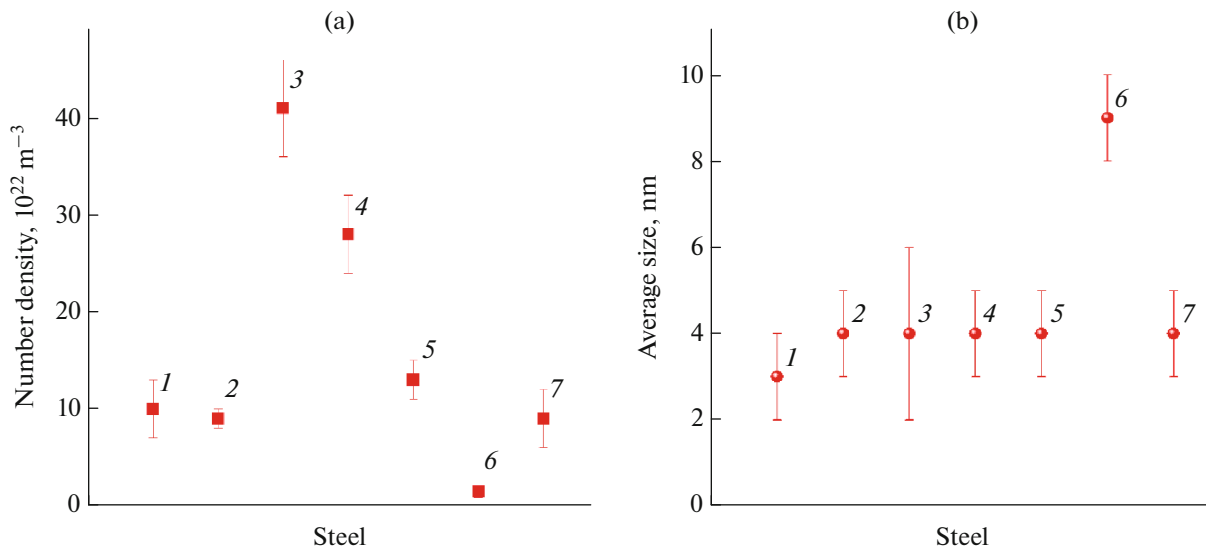


Fig. 5. (a) Number density and (b) average size of APT-detected oxide clusters in ODS steels: Eurofer ODS (1); 10Cr ODS (2); 14Cr ODS (3); Austenitic ODS (4); KP-3 ODS (5); KP-1 ODS (6); KP-4 ODS (7).

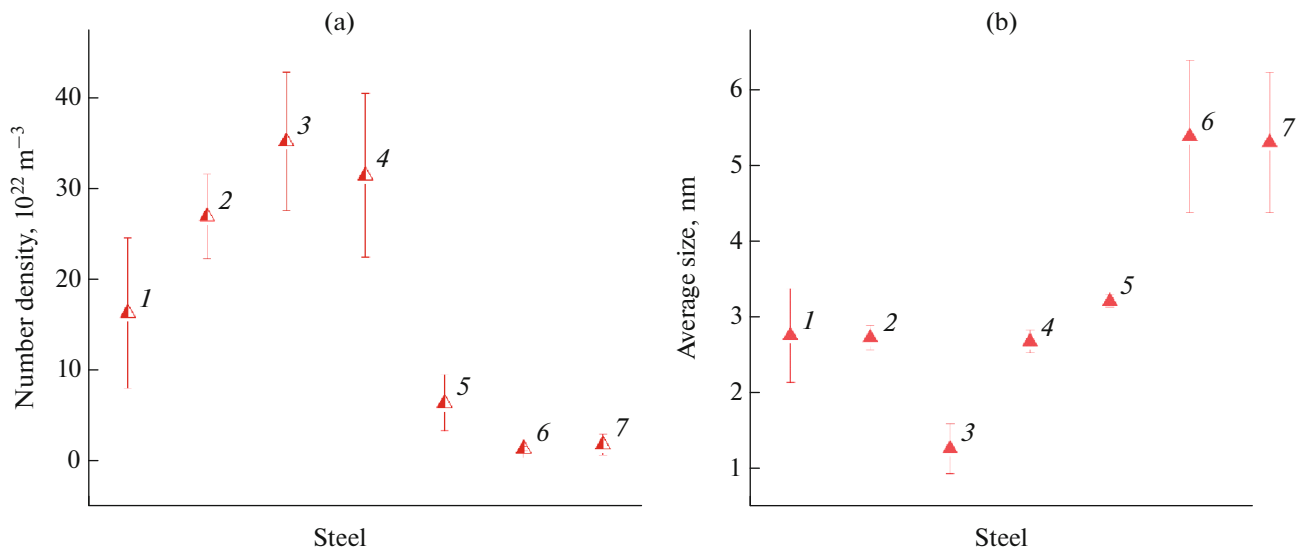


Fig. 6. (a) Number density and (b) average size of SAXS-detected inclusions in ODS steels: Eurofer ODS (1); 10Cr ODS (2); 14Cr ODS (3); Austenitic ODS (4); KP-3 ODS (5); KP-1 ODS (6); KP-4 ODS (7).

where σ_c is the contribution of clusters, σ_o is the contribution of oxide particles, σ_m is the solid-phase hardening, σ_{gb} is the contribution of grain boundaries.

To perform calculations, it is necessary to determine which type of inclusion is detected by TEM and APT. The most accurate average values are given by SAXS. If we assume that all objects detected by SAXS are oxides, we obtain the data presented in Fig. 7 (“direct calculation”), where the recalculation of hardening into hardness was performed using the for-

mula $H_v = 3\sigma_y$ [1]. The values closest to the results of microhardness measurement are obtained only for KP ODS steels. As noted earlier, other steels contain clusters in addition to oxide inclusions. By proportional correcting the number densities of oxide inclusions and clusters for SAXS measurements, we obtain the corrected data for the calculated hardness values (“corrected calculations,” Fig. 8). As can be seen from this figure, there is a fairly good agreement between the calculated hardness values and the results of microhardness measurement.

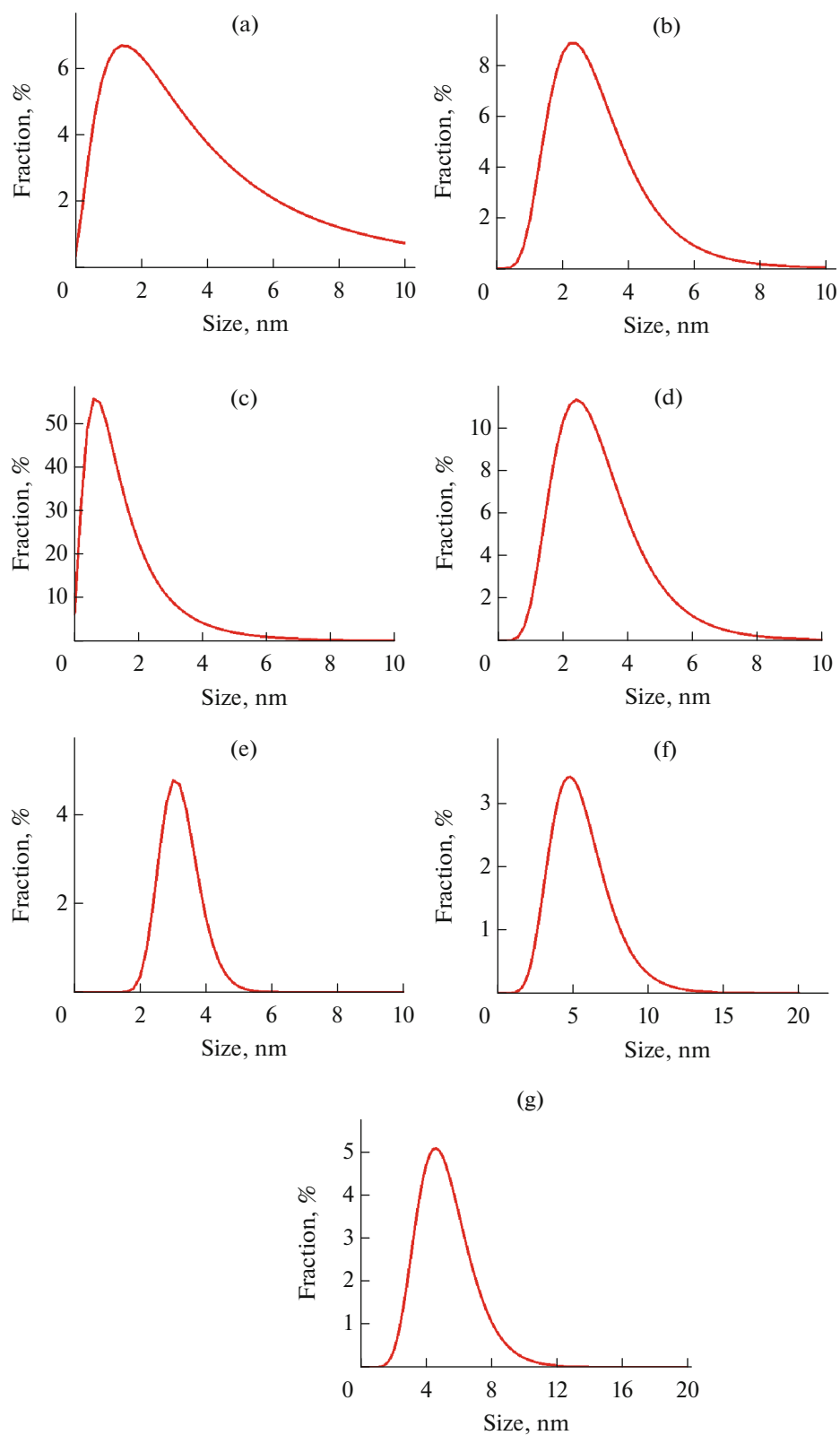


Fig. 7. Size distributions of nanoscale SAXS-detected inclusions in ODS steel samples: (a) Eurofer ODS; (b) 10Cr ODS; (c) 14Cr ODS; (d) Austenitic ODS; (e) KP-3 ODS; (f) KP-1 ODS; (g) KP-4 ODS.

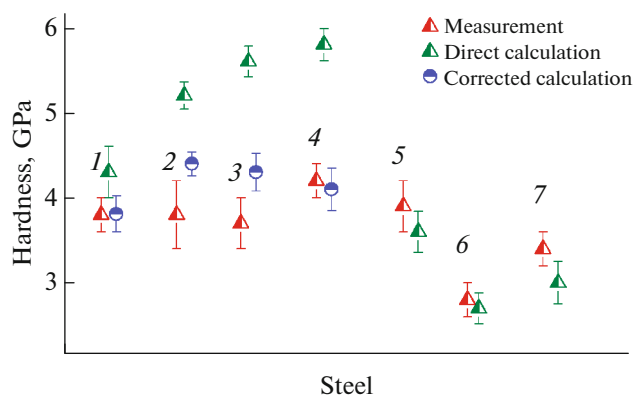


Fig. 8. Comparison of the results of direct microhardness measurement and DBH model calculations based on TEM, APT and SAXS data for ODS steels: Eurofer ODS (1); 10Cr ODS (2); 14Cr ODS (3); Austenitic ODS (4); KP-3 ODS (5); KP-1 ODS (6); KP-4 ODS (7).

DISCUSSION

The obtained data on the nanostructure of ODS steels is rather typical and widely presented in modern literature. However, many works rely on only one method of microscopy analysis: TEM, APT, small-angle neutron scattering, or SAXS. A comprehensive analysis of nanostructures was performed only in large projects. In [24], within the frame of the 7th European Framework Program (MatISSE project), ODS steels were studied by TEM, APT, small-angle neutron scattering and electron backscatter diffraction. The applied model with one type of oxide inclusions showed reasonable agreement between the calculated yield stress and the experimental yield stress of ODS steels [24]. Nevertheless, the calculated yield stress demonstrated some excess in comparison with the experimental data. It should be noted that in studied Fe9Cr and Fe14Cr ODS steels, the number density of inclusions detected by TEM was higher than that detected by APT. Our study of various ODS steels has shown both oxides inclusions in steels and nanoclusters enriched in Y, O, Ti, V or other elements. These inclusions (oxides and nanoclusters) have different barrier strength and, therefore, should be considered in calculations as different objects. In our study, we have shown that the model with one type of oxides inclusions can lead to an overestimation of the calculated yield stress, especially in steels with high number density of clusters detected by APT.

CONCLUSIONS

Seven ODS steels developed in Europe, Japan, and Korea were studied by transmission electron microscopy, atom probe tomography, and small-angle X-ray scattering. Microscopy analysis revealed a significant number of nanoscale inclusions. Simultaneous analysis of all the TEM, APT and SAXS data allows us to

conclude that different types of inclusions (either TEM oxide inclusions or APT clusters) are found in the Eurofer ODS, Austenitic ODS, 10Cr ODS, and 14Cr ODS. The density of objects observed by SAXS is consistent with the sum of densities of objects observed separately by TEM and APT. Only KP ODS steels contain objects that are detected simultaneously by all methods of analysis (TEM, APT and SAXS) with almost the same number density, which indicates their identity. These results are also confirmed by the comparison of hardening calculations for different inclusion types with direct measurements of the microhardness of these steels.

ACKNOWLEDGMENTS

The authors thank Dr. P. Vladimirov from the Karlsruhe Institute of Technology (Germany), Prof. A. Kimura from the Kyoto University (Japan) and Dr. T.K. Kim from the Korean Atomic Energy Research Institute (Republic of Korea) for providing samples of the ODS steels.

FUNDING

The work was supported financially by the Ministry of Science and Higher Education of the Russian Federation (Agreement no. 075-15-2021-1352). Tomographic atom probe analysis was performed using the equipment of the KAMIKS Shared Use Center (<https://ckp-rf.ru/ckp/502001/>) of the NRC “Kurchatov Institute.”

CONFLICT OF INTEREST

The authors declare that they have no conflicts of interest.

REFERENCES

1. B. Mouawad, X. Boulnat, D. Fabrègue, M. Perez, and Y. de Carlan, *J. Nucl. Mater.* **465**, 54 (2015). <https://doi.org/10.1016/j.jnucmat.2015.05.053>
2. S. V. Rogozhkin, A. A. Khomich, A. A. Bogachev, A. A. Nikitin, V. V. Khoroshilov, A. A. Lukyanchuk, O. A. Raznitsyn, A. S. Shutov, A. L. Vasiliev, and M. Yu. Presniakov, *Phys. At. Nucl.* **83**, 1425 (2020). <https://doi.org/10.1134/S2079562920010121>
3. N. Oono and S. Ukai, *Mater. Trans.* **59**, 1651 (2018). <https://doi.org/10.2320/matertrans.M2018110>
4. R. Coppola, M. Klimiankou, R. Lindau, R. P. May, and M. Valli, *Phys. B (Amsterdam, Neth.)* **350**, e545(2004). <https://doi.org/10.1016/j.physb.2004.03.148>
5. S. V. Rogozhkin, A. A. Aleev, A. A. Lukyanchuk, A. S. Shutov, O. A. Raznitsyn, and S. E. Kirillov, *Instrum. Exp. Tech.* **60**, 428 (2017). <https://doi.org/10.1134/S002044121702021X>
6. O. A. Raznitsyn, A. A. Lukyanchuk, A. S. Shutov, and S. V. Rogozhkin, *J. Anal. Chem.* **72**, 1404 (2017). <https://doi.org/10.1134/S1061934817140118>
7. A. A. Aleev, S. V. Rogozhkin, A. A. Lukyanchuk, A. S. Shutov, O. A. Raznitsyn, A. A. Nikitin,

- N. A. Iskandarov, O. A. Korchuganova, and S. E. Kirillov, Certificate of State Registration of a Computer Program No. 2018661876 (September 20, 2018).
<https://www1.fips.ru/ofpstorage/Doc/IZPM/RUNWC1/000/000/002/702/112/%D0%98%D0%97-02702112-00001/document.pdf>.
8. B. Gault, M. Müller, A. La Fontaine, M. P. Moody, A. Shariq, A. Cerezo, S. P. Ringer, and G. D. W. Smith, *J. Appl. Phys.* **108**, 044904 (2010).
<https://doi.org/10.1063/1.3462399>
 9. M. K. Miller and O. Ridge, *Rev. Sci. Instrum.* **78**, 031101 (2007).
<https://doi.org/10.1063/1.2709758>
 10. A. Cerezo and L. Davin, *Surf. Interface Anal.* **39**, 184 (2007).
<https://doi.org/10.1002/sia.2486>
 11. A. Guinier and G. Fournet, *Polym. Sci.* **19**, 594 (1955).
<https://doi.org/10.1002/pol.1956.120199326>
 12. M. Doucet, J.H. Cho, and G. Alina, *Zenodo* **1**, 1 (2017).
<https://doi.org/10.5281/zenodo.438138>
 13. G. E. Lucas, *J. Nucl. Mater.* **206**, 287 (1993).
[https://doi.org/10.1016/0022-3115\(93\)90129-M](https://doi.org/10.1016/0022-3115(93)90129-M)
 14. S. Xu, Z. Zhou, and H. Jia, *Steel Res. Int.* **90**, 1800594 (2018).
<https://doi.org/10.1002/srin.201800594>
 15. M. Klimenkov, R. Lindau, and A. Möslang, *J. Nucl. Mater.* **386**, 553 (2009).
<https://doi.org/10.1134/S1063778818120049>
 16. D. Bhattacharyya, P. Dickerson, G. R. Odette, S. A. Maloy, A. Misra, and M. Natsi, *Philos. Mag.* **92**, 2089 (2012).
<https://doi.org/10.1080/14786435.2012.662760>
 17. L. Hsiung, M. Fluss, S. Tumej, J. Kuntz, B. El-Dasher, M. Wall, B. Choi, A. Kimura, F. Willaime, and Y. Serruys, *J. Nucl. Mater.* **409**, 72 (2011).
<https://doi.org/10.1016/j.jnucmat.2010.09.014>
 18. N. H. Oono, S. Ukai, S. Hayashi, S. Ohtsuka, T. Kaito, A. Kimura, T. Torimaru, and K. Sakamoto, *J. Nucl. Mater.* **493**, 180 (2017).
<https://doi.org/10.1016/j.jnucmat.2017.06.018>
 19. P. Song, A. Kimura, K. Yabuuchi, P. Dou, H. Watanabe, J. Gao, and Y. Huang, *J. Nucl. Mater.* **529**, 151953 (2020).
<https://doi.org/10.1016/j.jnucmat.2019.151953>
 20. M. J. Swenson, C. K. Dolph, and J. P. Wharry, *J. Nucl. Mater.* **479**, 426 (2016).
<https://doi.org/10.1016/j.jnucmat.2016.07.022>
 21. E. Gil, N. Ordás, C. García-Rosales, and I. Iturriza, *Fusion Eng. Des.* **98**, 1973 (2015).
<https://doi.org/10.1016/j.fusengdes.2015.06.010>
 22. K. J. Han, T. S. Byun, D. T. Hoelzer, C. H. Park, J. Yeom, and Jae-Keun Hong, *Mater. Sci. Eng., A* **559**, 111 (2013).
<https://doi.org/10.1016/j.msea.2012.08.041>
 23. A. P. Gulyaev and N. A. Kozlova, in *Special Steels and Alloys: Collection of Works* (Metallurgiya, Moscow, 1966), **Vol. 46**, p. 58.
 24. A. Chauhan, F. Bergner, A. Etienne, J. Aktaa, Y. de Carlan, C. Heintze, D. Litvinov, M. Hernandez-Mayoral, E. Onorbe, B. Radiguet, and A. Ulbricht, *J. Nucl. Mater.* **495**, 6 (2017).
<https://doi.org/10.1016/j.jnucmat.2017.07.060>